Electronic Supporting Information

Single Molybdenum Center Supported on N-Doped Black Phosphorus as an Efficient Electrocatalyst for Nitrogen Fixation

Pengfei Ou[1], Xiao Zhou[1, 2], Fanchao Meng[1], Cheng Chen[1], Yiqing Chen[1], Jun Song[1, *]

[1] *Department of Mining and Materials Engineering, McGill University, Montreal H3A 0C5, Canada*

[2] *Institute of Mechanical Engineering, École Polytechnique Fédérale de Lausanne, Lausanne, Vaud CH-1015, Switzerland*

S1. SACs at single and double vacancies

There exist multiple other possible configurations as a Mo atom is anchored at single or double vacancies (i.e., reconstructed SV59, DV, and reconstructed DV585) in BP doped by multiple N atoms, as shown in Figure S1 (a)-(f). The binding energies of the resultant Mo_1N_3 structures at SV59 are -5.96 eV and -1.34 eV with reference to atomic Mo and bulk Mo, respectively. This suggests that a single Mo atom can be stably adsorbed by three unsaturated N atoms at SV59, with even stronger bonding than that at SV. Besides, we have also examined the adsorption energies of Mo_1N_4 at DV and DV585, with the binding energies being -4.77 and -4.68 eV with reference to atomic Mo, and -0.15 and -0.05 eV with reference to bulk Mo, respectively, which again suggests strong anchoring of Mo at those defects.

To examine the relative stabilities of various types of vacancies, we have calculated the formation energies of single and double vacancies. The lowest-energy point defect is a reconstructed double vacancy (DV585) with the formation energy of 1.57 eV, which is composed of two buckled pentagons and one octagon. The reconstructed single vacancy (SV59)

consisting of adjacent 9-fold and 5-fold rings exhibits the second lowest formation energy (1.77 eV). The single vacancy formed from direct removal of one P atom from the pristine BP exhibits a formation energy value of 2.21 eV. The calculated formation energies of these point defects are much lower than those in graphene[12]. Therefore, it is reasonable to expect them to form during the synthetic process. On the other hand, the formation energy of a regular DV is much higher, and as a result we do not consider it in the present study. It is worth noting that although the SV59 was theoretically predicted to be the most stable SV in BP,[1] the existence of SV has been confirmed experimentally utilizing a combination of low-temperature scanning tunneling microscopy/spectroscopy (STM/STS).[2] Consequently in the present study we put our main focus on the electrocatalytic reactions of Mo-based SACs at SV.

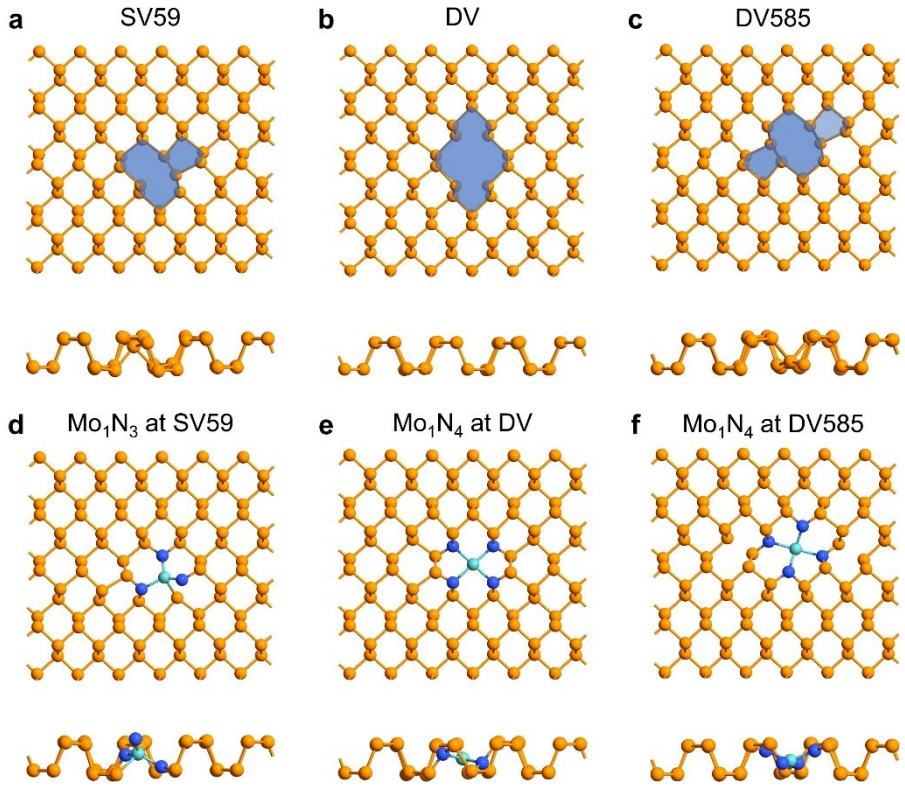

Figure S1. Top and side views of the optimized configurations of (a) SV59, (b) DV, and (c) DV585, as well as the Mo atom anchored at (d) SV59, (e) DV, and (f) DV585 in BP. The blue shaded areas in (a)-(c) present the defect regions. Blue, orange, and cyan balls represent doped N, P, and Mo atoms respectively.

S2. Kinetics of Mo migration out of SACs

The possible migration of Mo to escape SACs has been examined, which was found to generally exhibits a large energy barrier. For instance, the energy barrier for the adsorbed Mo atom at SV to migrate to a neighboring hollow site in N-doped BP is 14.6 eV, as illustrated in Figure S2. Such large kinetic energy barrier effectively renders the migration of Mo at the SAC a process unlikely to occur under ambient conditions.

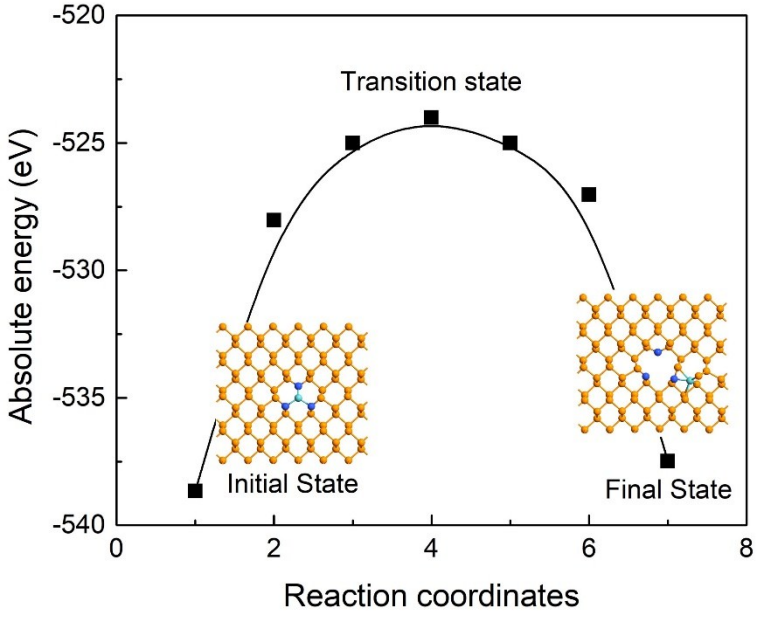

Figure S2. The minimum energy path (MEP) for the migration of an adsorbed Mo atom at SV in N-doped BP from the original defect binding site to a neighboring hollow site. Blue, orange, and cyan balls represent doped N, P, and Mo atoms respectively.

S3. Spin-resolved density state of N_2-adsorbed Mo_1N_3

The top and side views of the spin-resolved density states of the N_2-adsorbed Mo_1N_3 via side-on and end-on adsorptions are shown in Figure S3 (a) and (b) respectively, clearly illustrating that the charge clouds are localized and distributed on both the adsorbed N_2 and the Mo_1N_3 center. This suggest that N_2 be in indeed activated. Noteworthy is that the spin moments of side-on and end-on configurations are both changed to 1.00 μ_B after N_2 adsorption, and the energy differences between the spin-polarized and non-spin-polarized states are about -0.12 and -0.13 eV, respectively.

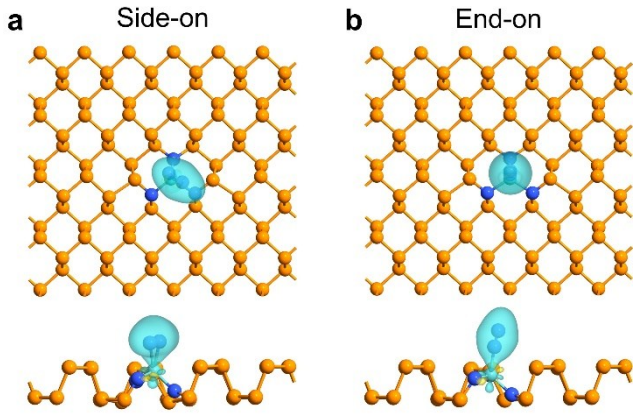

Figure S3. Top and side views of the optimized adsorption configurations and the spin-resolved density states of the (a) side-on and (b) end-on N_2 adsorption at Mo_1N_3 in BP. Blue, orange, and cyan balls represent doped N, P, and Mo atoms respectively. The cyan and yellow regions indicate the electron accumulation and depletion, respectively.

S4. Large Mo clusters as NRR electrocatalysts

In addition to the case of Mo SACs, we also studied the possibility of larger Mo clusters supported on phosphorus SV and DV585 in BP as potential NRR electrocatalysts. Considering the similar results obtained for SV and DV585, here we take the Mo_{13} cluster at SV as a representative example. Our calculations indicate that the calculated ΔE of adsorptions for $*N_2$, $*N_2H$, and $*NH_2$ species on the immobilized Mo_{13} cluster are -1.25, -4.21, and -1.73 eV, respectively (Figure S4). The corresponding N≡N bond length is also elongated to 1.14 Å. These results indicate that the Mo_{13} cluster sufficiently activates the inert N_2 molecule. However, the cluster shows a weak stabilization for the $*N_2H$ species ($\Delta G_{N_2-N_2H}$ = 0.82 > 0.5 eV), which consequently renders it unsuitable for N_2 reduction according the criteria outlined by Ling et al.[3] The above also implies that in application of Mo SACs in BP as NRR catalysts, it would be necessary to take measures to moderate or prevent Mo clustering which would have an adverse effect in the effectiveness.

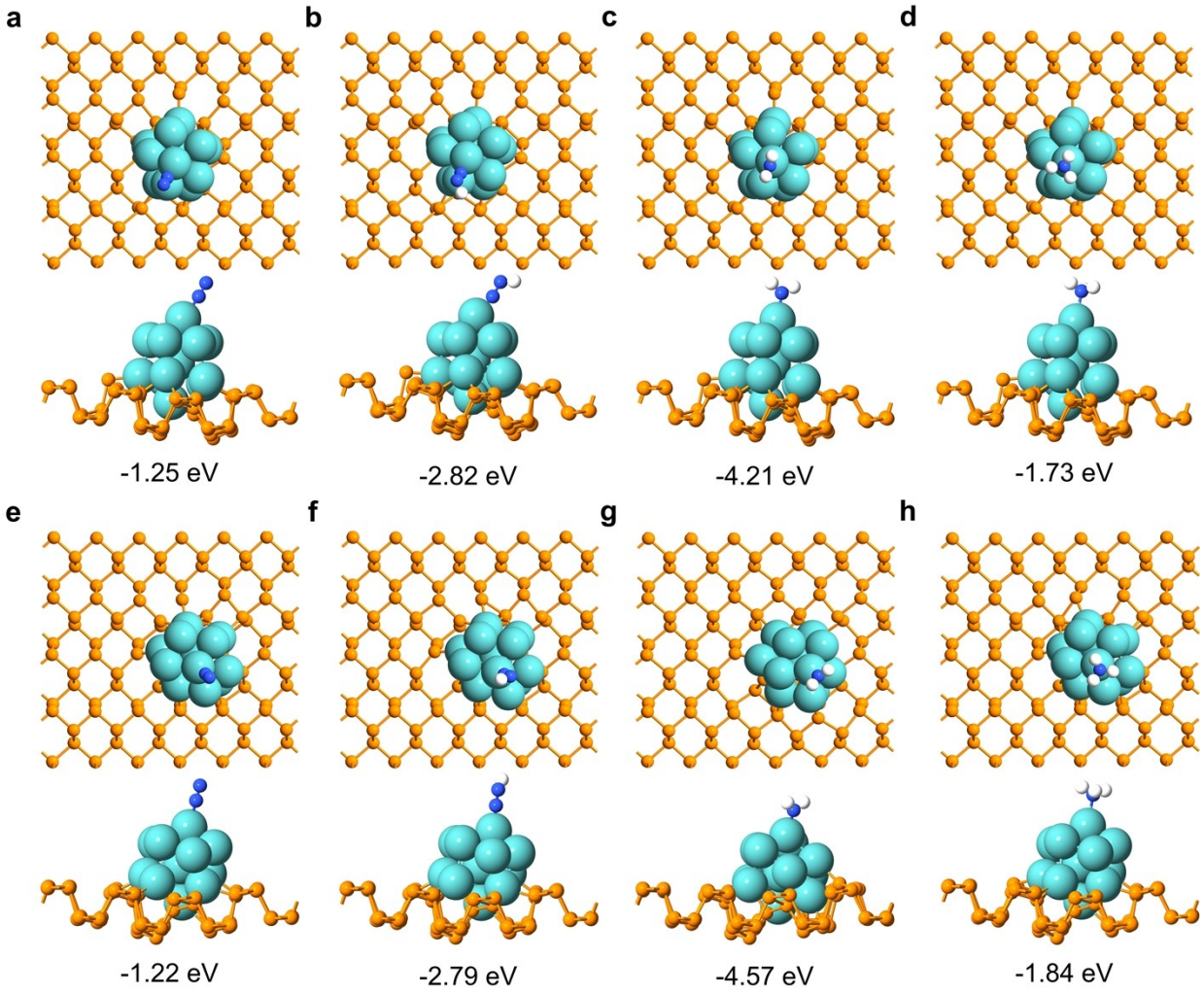

Figure S4. Top and side views of the optimized adsorption configurations and the corresponding adsorption energies of (a) $*N_2$, (b) $*N_2H$, (c) $*NH_2$, and (d) $*NH_3$ on Mo_{13} cluster at phosphorus SV and (e) $*N_2$, (f) $*N_2H$, (g) $*NH_2$, and (h) $*NH_3$ at phosphorus DV585 in BP. White, blue, orange, and cyan balls represent H, doped N, P, and Mo atoms respectively.

S5. Free energy diagrams for $Mo_1N_iP_{3-i}$ (i = 0, 1, and 2)

The free energy diagrams of $Mo_1N_iP_{3-i}$ (i = 0, 1, 2, or 3) for N_2 reduction to NH_3 via enzymatic, consecutive, alternating, and distal mechanisms at zero and applied potentials are summarized in Figures S5-9.

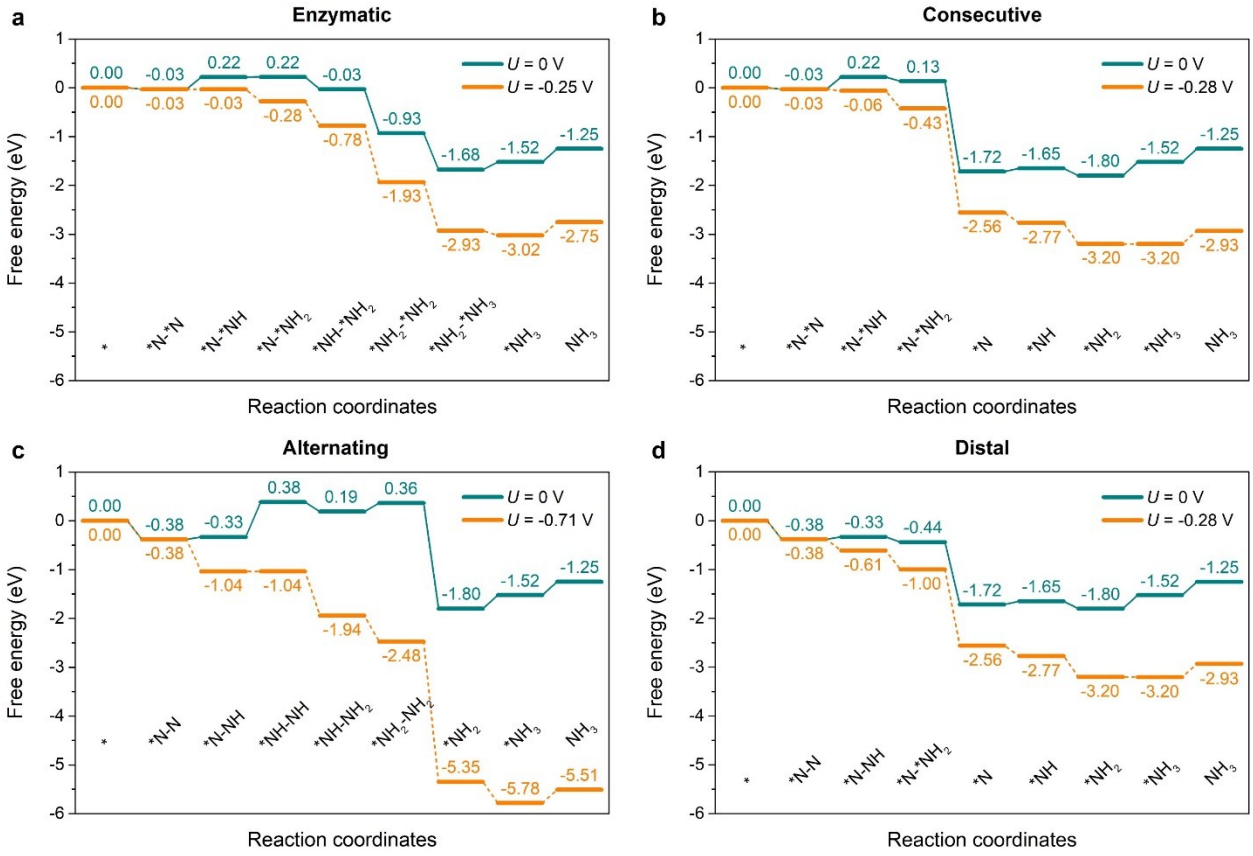

Figure S5. Free energy diagrams for N_2 reduction to NH_3 through (a) enzymatic, (b) consecutive, (c) alternating, and (d) distal mechanisms on sym_$Mo_1N_2P_1$ at zero and applied potentials. The green and orange curves respectively correspond to the situations of at 0 V and limiting potentials versus RHE, respectively.

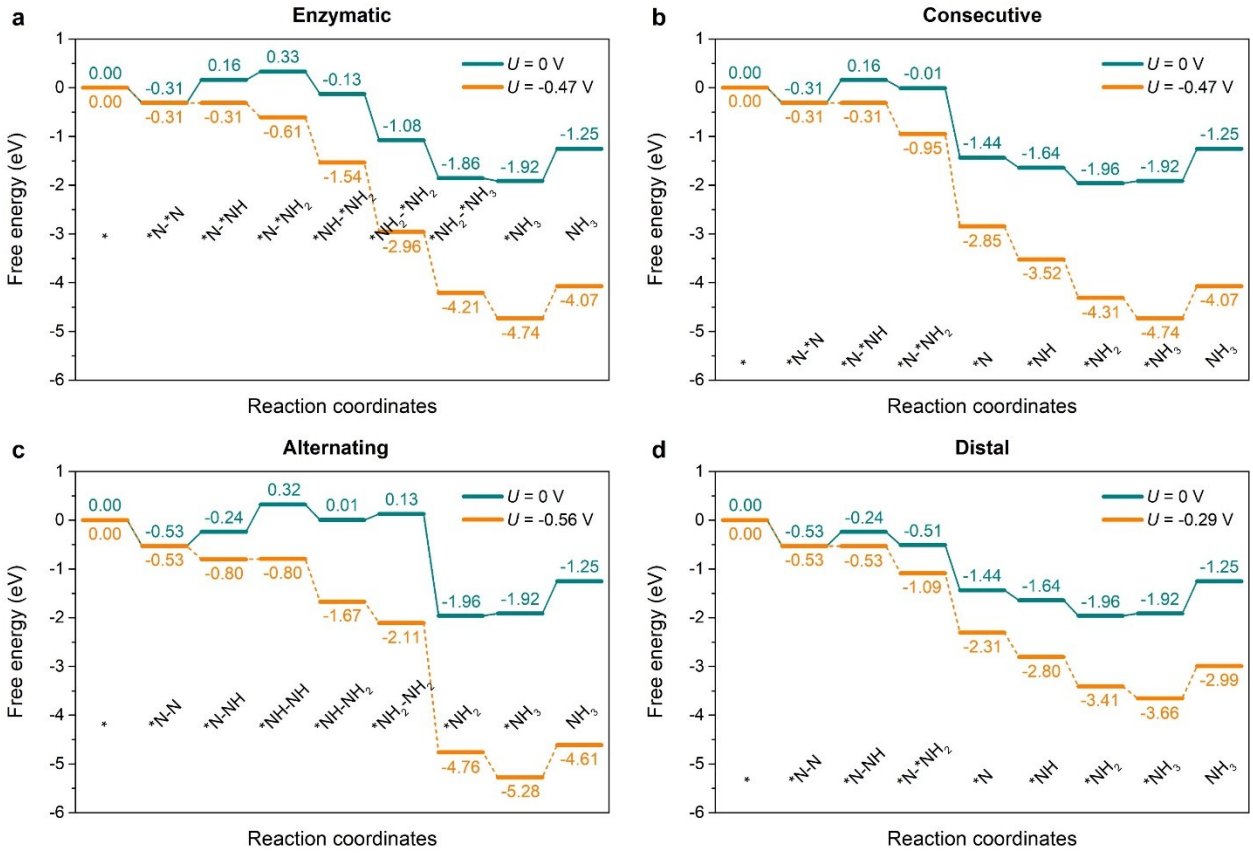

Figure S6. Free energy diagrams for N_2 reduction to NH_3 through (a) enzymatic, (b) consecutive, (c) alternating, and (d) distal mechanisms on asym_$Mo_1N_2P_1$ at zero and applied potentials. The green and orange curves respectively correspond to the situations of at 0 V and limiting potentials versus RHE, respectively.

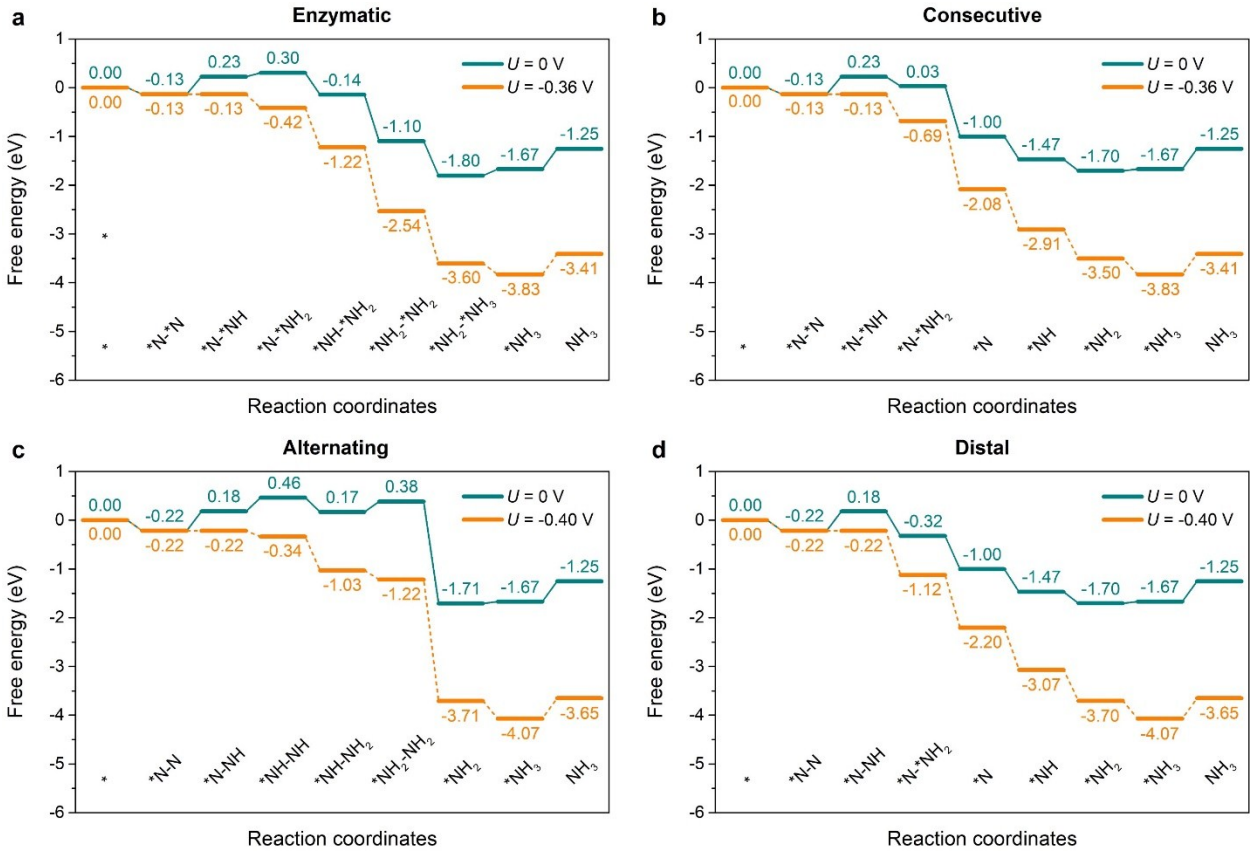

Figure S7. Free energy diagrams for N_2 reduction to NH_3 through (a) enzymatic, (b) consecutive, (c) alternating, and (d) distal mechanisms on sym_$Mo_1N_1P_2$ at zero and applied potentials. The green and orange curves respectively correspond to the situations of at 0 V and limiting potentials versus RHE, respectively.

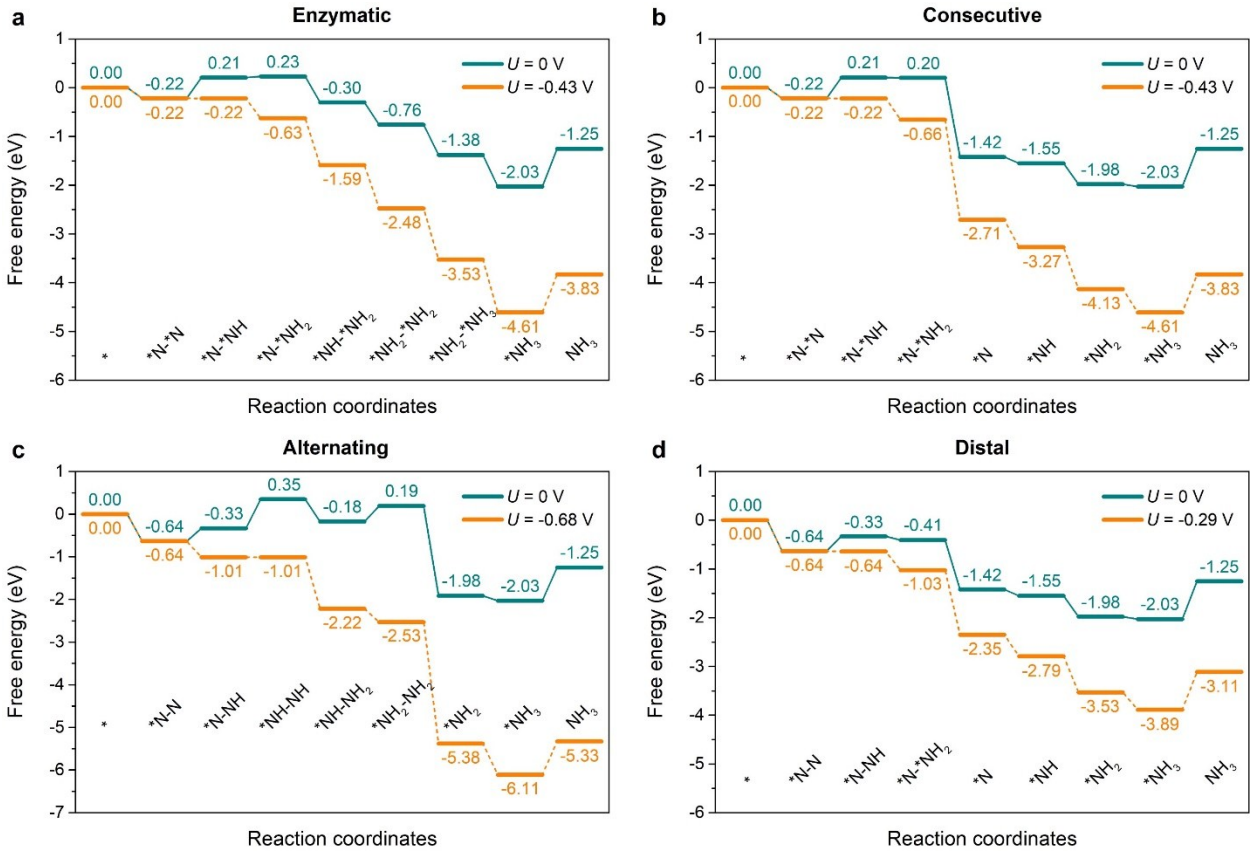

Figure S8. Free energy diagrams for N_2 reduction to NH_3 through (a) enzymatic, (b) consecutive, (c) alternating, and (d) distal mechanisms on asym_$Mo_1N_1P_2$ at zero and applied potentials. The green and orange curves respectively correspond to the situations of at 0 V and limiting potentials versus RHE, respectively.

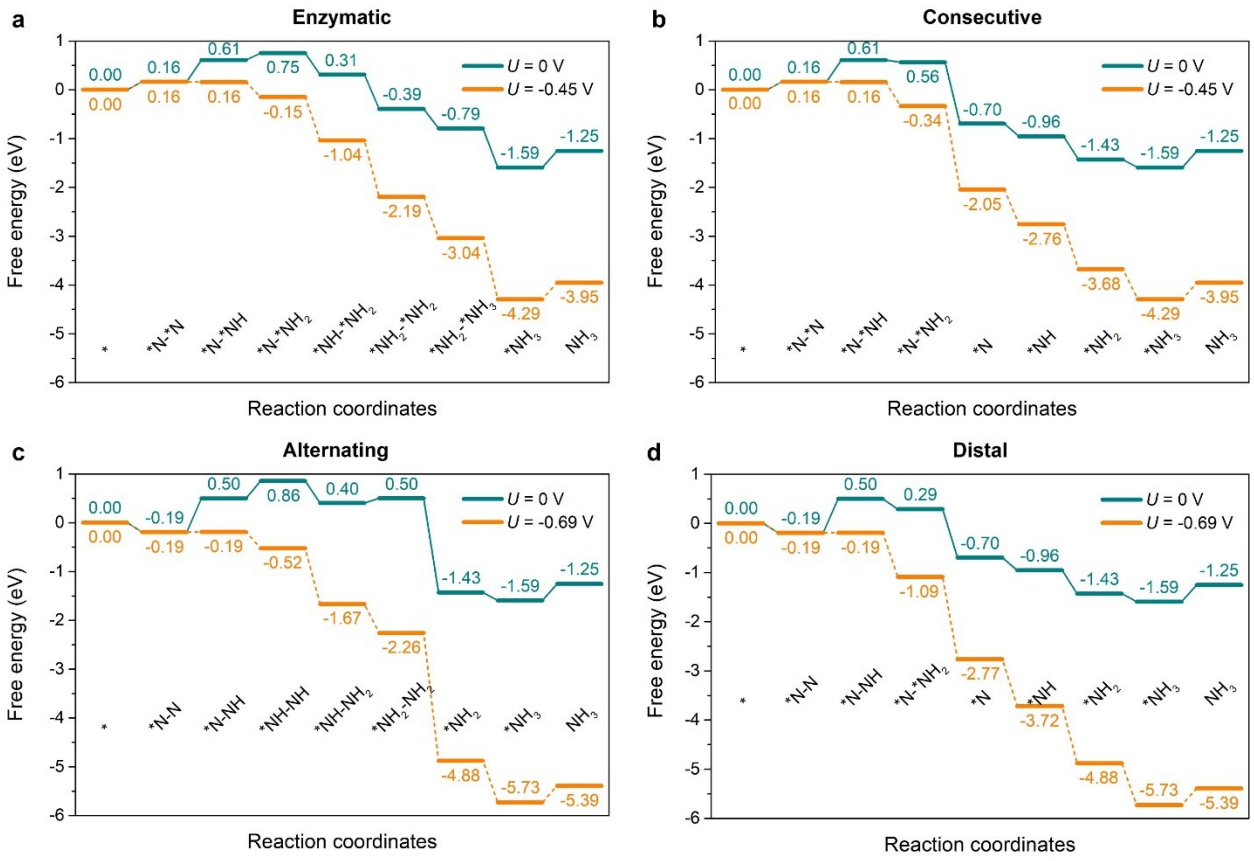

Figure S9. Free energy diagrams for N_2 reduction to NH_3 through (a) enzymatic, (b) consecutive, (c) alternating, and (d) distal mechanisms on Mo_1P_3 at zero and applied potentials. The green and orange curves respectively correspond to the situations of at 0 V and limiting potentials versus RHE, respectively.

References

1. Li, X.-B.; Guo, P.; Cao, T.-F.; Liu, H.; Lau, W.-M.; Liu, L.-M., Structures, Stabilities, and Electronic Properties of Defects in Monolayer Black Phosphorus. *Scientific reports* **2015**, *5*, 10848.
2. Guo, Y.; Robertson, J., Vacancy and Doping States in Monolayer and Bulk Black Phosphorus. *Scientific reports* **2015**, *5*, 14165.
3. Ling, C.; Ouyang, Y.; Li, Q.; Bai, X.; Mao, X.; Du, A.; Wang, J., A General Two-Step Strategy–Based High-Throughput Screening of Single Atom Catalysts for Nitrogen Fixation. *Small Methods* **2018**, 1800376.